Modeling global radiative effect of brown carbon: A larger heating source in the tropical free troposphere than black carbon

Aoxing Zhang[1], Yuhang Wang[1], Yuzhong Zhang[1,2], Rodney J Weber[1], Yongjia Song[1], Ziming Ke[1,3], Yufei Zou[1,4]

5   [1]School of Earth and Atmospheric Sciences, Georgia Institute of Technology, Atlanta, USA
[2]Now at School of Engineering and Applied Sciences, Harvard University, Cambridge, MA, USA
[3]Now at Department of Atmospheric Science, University of Wyoming, Laramie, Wyoming, USA
[4]Now at School of Environmental and Forest Sciences, University of Washington, Seattle, WA, USA

10   *Correspondence to*: Yuhang Wang (yuhang.wang@eas.gatech.edu)

Abstract. Carbonaceous aerosols significantly affect global radiative forcing and climate through absorption and scattering of sunlight. Black carbon (BC) and brown carbon (BrC) are light-absorbing carbonaceous aerosols. The direct radiative effect (DRE) of BrC is uncertain. A recent study suggests that BrC absorption is comparable to BC in the upper troposphere over biomass burning regions and that the resulting radiative heating tends to stabilize the atmosphere. Yet current climate

15   models do not include proper physical and chemical treatments of BrC. In this study, we derived a BrC global biomass burning emission inventory on the basis of the Global Fire Emissions Database 4 (GFED4), developed a BrC module in the Community Atmosphere Model version 5 (CAM5) of Community Earth System Model (CESM) model, and investigated the photo-bleaching effect and convective transport of BrC on the basis of Studies of Emissions, Atmospheric Composition, Clouds and Climate Coupling by Regional Surveys (SEAC⁴RS) and Deep Convective Clouds and Chemistry Project (DC3)

20   measurements. The model simulations of BC were also evaluated using HIAPER (High-Performance Instrumented Airborne Platform for Environmental Research) Pole-to-Pole Observations (HIPPO) measurements. We found that globally BrC is a significant absorber, the DRE of which is 0.10 W/m², more than 25% of BC DRE (+0.39 W/m²). Most significantly, model results indicated that BrC atmospheric heating in the tropical mid and upper troposphere is larger than that of BC. The source of tropical BrC is mainly from wildfires, which are more prevalent in the tropical regions than higher latitudes and release

25   much more BrC relative to BC than industrial sources. While BC atmospheric heating is skewed towards northern mid-latitude lower atmosphere, BrC heating is more centered in the tropical free troposphere. The contribution of BrC heating to the Hadley circulation and latitudinal expansion of the tropics is comparable to BC heating.

1 Introduction

30   Carbonaceous aerosols, including black carbon (BC) and organic carbon (OC), are important factors in global atmospheric radiative forcing. BC warms the atmosphere by directly absorbing solar radiation (Bond et al., 2013). OC used to be thought

to cool the atmosphere due to its light scattering properties. However, some OC, known as "brown carbon" (BrC), absorbs visible light with a wavelength dependence; the efficiency increases rapidly with decreasing wavelength (Hecobian et al., 2010; Kirchstetter and Thatcher, 2012; Kirchstetter et al., 2004; Yang et al., 2009).

The primary source of BrC is incomplete combustion of biomass and biofuel (Chakrabarty et al., 2010; Feng et al., 2013; Desyaterik et al., 2013; Washenfelder et al., 2015). There is evidence that BrC is also associated with fossil fuel combustion and urban emissions (Zhang et al., 2011; Costabile et al., 2017; Yan et al., 2017; Xie et al., 2017). Secondary BrC is mainly produced from the photo-oxidation of volatile organic compounds (VOCs), such as nitrophenols and aromatic carbonyls (Jacobson, 1999; Nakayama et al., 2010; Nakayama et al., 2013), monoterpenes (Laskin et al., 2014), and methylglyoxal (Sareen et al., 2013). Secondary BrC also comes from aqueous-phase reactions in droplets (Updyke et al., 2012; Nguyen et al., 2012) and homogenous and heterogenous reactions of catechol (Pillar et al., 2014; Pillar and Guzman, 2017; Magalhães et al., 2017) and phenolic compounds (Yu et al., 2016; Lavi et al., 2017; Smith et al., 2016). BrC from biomass burning contributes more to light absorption than the other sources (Chakrabarty et al., 2010; Saleh et al., 2014; Kirchstetter and Thatcher, 2012; McMeeking, 2008). Factor analysis of water-soluble organic carbon (WSOC) over the southeastern United States averaged for one year (Hecobian et al., 2010) attributed ~50% of solar absorption at 365 nm to biomass burning emissions, 20-30% to secondary organic carbon, and ~10% to primary urban emissions (mobile sources).

Alexander et al. (2008) analyzed the radiative effects of aerosols in the outflow region of East Asia and found that wood smoke BrC accounted for 14% of total aerosol absorption. Liu et al. (2014) found a ~20% reduction of aerosol cooling from BrC absorption at the top of the atmosphere on the basis of measured BrC vertical profiles. However, current observations do not provide enough constraints on the global BrC radiative forcing (Schuster et al., 2016a; Schuster et al., 2016b).

Global models have been applied to estimate Direct Radiative Forcing (DRF) and Direct Radiative Effects (DRE) of BrC. Aerosol DRE represents the difference of radiative budget with and without aerosols, and DRF represents the difference of DRE between present day and pre-industrial times (Heald et al., 2014). The study by Feng et al. (2013) suggested a +0.04-0.11 W/m^2 warming effect at the top of atmosphere due to the absorption of BrC, and attributed 19% of anthropogenic aerosol absorption to BrC. Wang et al. (2014) estimated the global DRF of +0.11 and +0.21 W/m^2 for BrC and BC, respectively. Jo et al. (2016) estimated a BrC DRE of +0.11 W/m^2. Lin et al. (2014) estimated a BrC DRE of +0.22-0.57 W/m^2, which accounted for 27%-70% of the BC absorption in their model. Park et al. (2010) modeled BrC over East Asia and calculated a DRE of +0.05 W/m^2 at the top of the atmosphere. Brown et al. (2018) estimated a BrC DRE of +0.13±0.01 W/m^2 and 0.01± 0.04 W/m^2 from BrC aerosol-cloud interaction. Saleh et al. (2015) estimated a BrC DRE of 0.22 W/m^2 when BrC externally mixed with BC, and 0.12 W/m^2 when BrC is internally mixed with BC. All of these model estimations of BrC DRE and DRF treated BrC similar to BC, where properties were invariant with atmospheric processing or aging.

65

In this study, we developed and implemented a BrC module in the Community Earth System Model (CESM) to assess the effects of BrC DRE. Laboratory and field studies showed a reduction of BrC absorption when exposed to light, which is usually referred to as "photo-bleaching" (Zhao et al., 2015). A recently global model simulation (Wang et al., 2018) included this effect, resulting in a large reduction of global BrC DRE to +0.048 W/m^2 compared to previous estimates from the

70 studies listed above. et al. (2018) also showed a reduction of BrC DRE to 0.06±0.008 W/m^2 because of photo-bleaching. Other effects of atmospheric processing have not yet been in BrC global modeling. Results from the Deep Convective Clouds and Chemistry Project (DC3) found high concentrations of BrC in the continental upper tropospheric due to convective transport, suggesting more efficient atmospheric vertical transport of BrC than previously assumed (Zhang et al., 2017). Here, we include these effects and make use of the aircraft measurements of BrC absorption profiles from DC3 and

75 SEAC[4]RS campaigns to evaluate the model formulation and simulation results. The global BrC emissions from biomass burning, biofuel emissions, and secondary formation were included. We tested the sensitivity of photo-bleaching effect and the deep convective transport of BrC to its DRE, and estimated the global DRE. This is the first attempt to comprehensively analyze how convective transport and photo-bleaching affect global atmospheric heating by BrC absorption relative to BC.

2 Model Description

80 ### 2.1 The CESM Model

We developed the brown carbon simulation based on the Community Earth System Model (CESM) version 1.2.2 and its atmospheric component, the Community Atmosphere Model version 5 (CAM5) (Neale et al., 2010). The CAM5 model has a comprehensive mechanism for aerosols and cloud-aerosol interaction (Liu et al., 2012; Ghan et al., 2012; Gettelman et al., 2010). The CAM5 radiation scheme is the Rapid Radiative Transfer Method for GCMs (RRTMG), which provides an

85 accurate method for radiative flux calculation (Iacono et al., 2008; Mlawer et al., 1997). The atmospheric chemistry module, turbulence scheme, convection scheme, and cloud physics are coupled in the model (Zhang and McFarlane, 1995; Bretherton and Park, 2009; Park and Bretherton, 2009; Richter and Rasch, 2008; Morrison and Gettelman, 2008). We used a 3-mode version of the modal aerosol model (MAM-3) for aerosol modeling in CAM5. The 3 modes are Aitken, accumulation, and coarse modes (Neale et al., 2010). In our BrC simulations, we used CAM5 with a spatial resolution of 1.9°x2.5°. The wet

90 scavenging scheme of aerosols in CAM5 includes below-cloud scavenging and in-cloud scavenging, which was found to have a high bias (Wang et al., 2011; Liu et al., 2012)., we nudged CAM5 meteorological field (temperature, humidity, wind, surface pressure and heat) to GEOS-5.2.0 meteorological data products (Suarez et al., 2008) every 6 hours in order to evaluate the model simulations with BrC observations (Ma et al., 2013; Chipperfield, 2006). We also conducted 5-year free-running model simulations to analyze the climate response to BrC and BC heating. The spin-up time is 3 months in the

95 nudged CAM5 simulations and is 1 year in the free-running simulations.

2.2 Emissions

We derived global BrC emissions from biomass burning, biofuel, and secondary formation. Same as Brown et al., 2018, we used the parameterization by Saleh et al. (2014) for biomass and biofuel burning, in which emitted BrC absorption is a function of BC/Organic Aerosols (OA) emission ratio. We included secondary aerosols from the oxidation of aromatic as the major source of secondary BrC (Hecobian et al., 2010; Sareen et al., 2013; Lin et al., 2015). Secondary BrC produced from aromatic oxidation absorbs more solar radiation in high-NOx conditions (Laskin et al., 2015; Lin et al., 2015; Liu et al., 2012; Nakayama et al., 2010, 2013; Yu et al., 2014; Zhong and Jang, 2011). We did not consider the NOx dependence of secondary BrC in this study. More details will be described in section 3.

The biomass burning emissions we used are from the Global Fire Emission Database version 4 including small fires (GFED4s) (Giglio et al., 2013; Randerson et al., 2012). It contains global burned area distribution and biomass burning emission factors of related aerosols and gas species for different fire types, with a spatial resolution of 0.25°x0.25°. In CAM5, we aggregated it to a spatial resolution to 1.9°x2.5° and used GFED daily emission and diurnal cycle factors. Fire emissions can reach high altitudes (e.g., Neale et al., 2010). We used an observation-constrained global fire plume rise dataset in which MODIS fire hotspot and fire radiance power data were used in a 1-D fire plume rise model and the resulting fire plume distribution is in good agreement with the Multi-angle Imaging SpectroRadiometer (MISR) observations (Ke, 2019). Biomass burning emissions have high uncertainties caused by burned area, emission factors, fuel loads and combustion completeness factors (Akagi et al., 2011; Giglio et al., 2013), and the complex interactions between fire, terrestrial ecosystem, and climate systems amplify these uncertainties (Zou et al., 2019).

Anthropogenic emissions are from the IPCC AR5 emission dataset (Lamarque et al., 2010), and BC and OC emissions are updated based on the emission inventory of 2000 (Bond et al., 2007; Junker and Liousse, 2008). We increased anthropogenic emissions in China by 50% according to Zhang et al. (2009). For the Arctic region (> 66°N), we used the Evaluating the Climate and Air Quality Impacts of Short-lived Pollutants (ECLIPSE) emission dataset, which includes an improvement for the Arctic BC emissions (Stohl et al., 2013; Klimont et al., 2015).

3 Brown Carbon Module

3.1 BrC optical property and photo-bleaching

BrC absorption depends on its Mass Absorption Efficiency (MAE), which is the ratio of light absorption in the wavelength λ to BrC mass concentration ($m^2 g^{-1}$):

$$MAE_{BrC}(\lambda) = \frac{A(\lambda)}{c_{BrC}} . \tag{1}$$

where $A(\lambda)$ represents the absorption of BrC at the wavelength of λ (m^{-1}), and c_{BrC} is the mass concentration of BrC (g m^{-3}).

130   We used a constant MAE value for primary BrC, 1.0 m^2/g at 550 nm (McMeeking, 2008). There are other MAE estimates such as 3.6-4.1 m^2/g (Alexander et al., 2008) and 0.58-0.64 m^2/g (Hecobian et al., 2010). MAE value may also change in different seasons (Cheng et al., 2011). At present, there are not enough observations to specify variable MAE values in the model. We used an MAE value of 1.5 m^2/g at 365 nm for secondary BrC based on the work by Nakayama et al. (2010). The MAE value at the other wavelengths was calculated using the following function (Bond and Bergstrom, 2006):

135   $$MAE(\lambda) = MAE(\lambda_0) * (\lambda_0/\lambda)^{AAE}, \tag{2}$$

where AAE is absorption Ångström exponent, and λ_0 is 550 and 365 nm for primary and secondary BrC, respectively. We used AAE = 5.0 for λ < 2 μm (Jo et al., 2016). In the CESM RRTMG model, the imaginary part of refractive index is 0.0050 in the band of 442 nm to 625 nm for non-absorbing OC. Its value for BrC is estimated using the following equation:

$$k_{BrC,\lambda} = k_{OA,\lambda} * \frac{c_{OA}}{c_{BrC}} = \frac{\rho\lambda \cdot A(\lambda)}{4\pi \cdot c_{BrC}} = \frac{\rho\lambda \cdot MAE(\lambda)}{4\pi}, \tag{3}$$

140   The estimated k_{BrC} value is 0.045 at 550 nm for primary BrC and 0.043 at 365 nm for secondary BrC, respectively.

There is observational evidence that both primary and secondary BrC are affected by photochemical aging (or bleaching), which reduces BrC light absorption when exposed to light (Forrister et al., 2015; Sareen et al., 2013; Lee et al., 2014; Zhong and Jang, 2011; Wong et al., 2017; Wong et al, 2019). Different components of SOA have different photo-bleaching

145   lifetimes. Aromatic SOA has a half-life of 12-24 hours (Liu et al., 2016; Lee et al., 2014; Zhong and Jang, 2011), limonene SOA has a half-life of <0.5 hours (Lee et al., 2014). Methylglyoxal SOA has a half-life of 90 minutes (Zhao et al., 2015; Wong et al., 2017). Therefore, we specify a decay half-life of 12 hours for primary BrC in the daytime until 6% is left and no further photobleaching occurs (Forrister et al., 2015) due to stable high molecular weight chromophores (Di Lorenzo and Young, 2015; Di Lorenzo et al., 2017; Wong et al., 2017; Wong et al, 2019). The half-life for secondary aromatic BrC is

150   specified at 12 hours in daytime (Liu et al., 2016). The other secondary BrCs that have shorter lifetimes contribute little to global radiative forcing and are not included in the model.

The analysis of aircraft BrC observations by Zhang et al. (2017) showed that BrC transported by deep convection plays a significant role in radiative heating of the upper troposphere, and that BrC warming is about one third of BC warming at the

155   tropopause. The standard model simulations show a large low bias of BrC in the upper troposphere compared to the observations by Zhang et al. (2017). In addition, in-cloud heterogeneous BrC production is another possible reason for the high level BrC in the upper troposphere. A fraction of biomass burning BrC from heterogeneous oxidation by ozone will stay free from bleaching, and BrC from heterogeneous oxidations by OH has a long lifetime of days (Browne et al., 2019). Therefore, we conducted sensitivity simulations of BrC to investigate the effects of photo-bleaching and wet scavenging

160   during deep convection.

3.2 BrC Emissions

We assumed that BrC is emitted in the accumulation mode (Liu et al, 2013). Sources of the more stable forms of BrC include primary emissions of biomass burning and biofuel, as well as secondary formation from aromatic oxidation. Biomass burning BrC emissions were parameterized as a function of BC to OA ratio of the emissions (Saleh et al., 2014):

165
$$k_{OA,550} = 0.016 log_{10}\left(\frac{E_{BC}}{E_{OA}}\right) + 0.03925, \tag{4}$$

where $k_{OA,550}$ is OA absorptivity at 550 nm, and E_{BC} and E_{OA} are BC and OA emission rates (g m^{-2} s^{-1}), respectively. We scaled BrC Emissions based on $k_{OA,550}$, MAE and OA emissions using the following equation by Liu et al. (2013):

$$E_{BrC} = \frac{4\pi k_{OA,550} \cdot E_{OA}}{\rho \cdot 550nm \cdot MAE_{BrC}(550\ nm)}. \tag{5}$$

where ρ is particle density (g m^{-3}), and E_{BrC} is BrC emission rate (g m^{-2} s^{-1}).

170

Using the GFED emissions inventory, we estimated an annual average global BrC source from biomass burning of 3.6 TgC/yr, ~23% of OC emissions (15.9 TgC/yr) and about twice as large as BC emissions (1.9 TgC/yr). Using the same equations and an average E_{BC}/E_{OA} ratio of 0.41 (Junker and Liousse, 2008), we estimated an E_{BrC}/E_{OA} ratio of 0.38 and an annual global BrC biofuel source of 3.1 TgC/yr on the basis of biofuel emission inventory by Bond et al. (2007). The estimates of primary BrC emissions are comparable to previous studies (Table 1). BrC emissions from fossil fuel combustion are not yet well characterized to be included in a global model (Saleh et al., 2014; Xie et al., 2017).

The major fraction of secondary BrC that affects atmospheric heating is formed during the oxidation of aromatics (Jacobson, 1999; Nakayama et al., 2013; Zhong et al., 2012). As in previous studies (Jo et al., 2016; Wang et al., 2014), we assumed that secondary BrC is from aged aromatic SOA. In the CAM5 MAM aerosol mechanism, the SOA mass yield for aromatics oxidation is 15% (Neale et al., 2010; Odum et al., 1997). We estimated a global secondary BrC source of 4.1 TgC/yr in agreement with previous studies.

BrC emissions used in this study and the comparison to previous studies are summarized in Table 1, and the emission distribution is shown in Figure 1. Biofuel emissions are high in China and India, and secondary BrC sources are also large in Europe and North America. Figure 2 shows the annual cycle of BrC emissions in 2010. Biofuel and secondary BrC sources have little seasonal variation in the model, while biomass burning has significant seasonal variation. The BrC source is the highest in August at 18.9 TgC/yr. Biomass burning emission accounts for more than 60% of the BrC emissions in August.

4 Model evaluation

4.1 Black carbon measurements from HIAPER

HIAPER (High-Performance Instrumented Airborne Platform for Environmental Research) Pole-to-Pole Observations (HIPPO) measured atmospheric composition approximately from the Arctic to the Antarctic over the Pacific Ocean (Wofsy, 2011). HIPPO executed 5 missions from January 2009 to September 2011. The flight path of each HIPPO mission is shown in Figure 3. Measurements over continental North America east of 140°W were not included in our model evaluation. BC measurements for particles with a size range of 90-600 nm were made from a single-particle soot photometer (SP2) and we increased measured BC data by a factor of 1.1 to account for larger sized BC in the model evaluation (Schwarz et al., 2010; Schwarz et al., 2013). We make use of HIPPO BC measurements to constrain convective transport and wet scavenging.

Wet scavenging is uncertain in 3-D global modelling of BC (Schwarz et al., 2010; Liu et al., 2011). Wang et al. (2013) tested the sensitivities of different physical mechanisms and found a high sensitivity of BC simulations to convective transport and wet removal. Comparison of CAM5 BC simulations with HIPPO observations in Figure 4 shows large overestimates of BC in the tropics and the upper troposphere. Since the emissions of BC are from the surface, the model high biases in these regions suggest insufficient wet scavenging during convection. We therefore increased interstitial BC scavenging by a factor of 5 to increase wet scavenging and decrease simulated BC concentrations in the tropics. The high biases above 300 hPa at mid and high latitudes persisted particularly for HIPPO-1 in January 2009 and HIPPO-2 in November 2009. In winter, the simulated high BC concentrations were above the tropopause level at mid and high latitudes, indicating that convective transport reached too high an altitude. We therefore limited deep convection mass transport to an altitude of 50 hPa below the model estimated tropopause, after which the high biases at mid and high latitudes above 200 hPa were corrected. During HIPPO-3 in March-April 2010, model simulated free tropospheric BC at northern mid and high latitudes were much lower than the observations, suggesting excessive scavenging in the model. We reduced cloud-born BC scavenging to 10% when cloud ice is present and to 50% for the other conditions, which improved the model simulations of free tropospheric BC simulations at mid and high latitudes in HIPPO-3 (and HIPPO-2). The modification slightly worsened the model high bias at northern mid and high latitudes in the summer for HIPPO-5 in August-September 2011 and to a lesser extent for HIPPO-4 in June-July, 2011. Overall, the modified CAM5 model simulates HIPPO BC observations much better than the original version.

4.2 Aerosol optical depth over fire emission dominated regions

Direct assessments of BrC sources using observations are difficult because of limited observations. We can, however, evaluate model simulations of fire aerosols with AOD measurements. For this purpose, we chose the months and regions in model simulations that >50% of monthly mean AOD data are from fire emissions for 2010. The distribution of model simulated mean AOD for data points selected in this manner are shown in Figure S1(a). For comparison purpose, the

ground-based AOD measurements were obtained from the Aerosol Robotic Network (AERONET) (Holben et al., 1998). To compare with model simulated AOD data at 550 nm, the AOD measurements at 500 and 675 nm were used to compute Ångström exponent (Ångström, 1964) and calculate the corresponding AOD values at 550 nm (Kumar et al., 2013). Figure 5(a) compares the monthly mean fire dominated 550 nm AOD observations in 2010 in AERONET with corresponding
225   monthly mean model results for selected months and regions. The correlation coefficient, r, is high at 0.88, although the observed AOD data were underestimated implying a low bias in fire emissions.

We also compared AOD with the measurements from Moderate Resolution Imaging Spectroradiometer (MODIS) on Terra (EOS-AM-1) satellite for the months and regions in model simulations that >50% of monthly mean AOD data are from fire
230   emissions for 2010. We used Collection 6 of MODIS level-3 Deep Blue/Dark Target merged product with a resolution of 1°x1° (Platnick et al., 2017). Figure 5(b) shows the comparison. The correlation coefficient, r, is lower at 0.67 than the comparison with AERONET observations. One reason is that the high AOD data in the outflow region of the tropical Atlantic from fire emissions over Africa were significantly underestimated (Figure S1(b)); similar low biases were also found in the outflow region of fire emissions in South America. Additionally, CAM5 underestimates AOD at high latitudes
235   (Liu et al., 2012). The general low bias of fire aerosol emissions was also found by Ward et. al. (2012).

5 Results

5.1 Model simulations of BrC for DC3 and SEAC[4]RS missions

We evaluated BrC model simulations using the measured BrC absorption data from Studies of Emissions, Atmospheric
240   Composition, Clouds and Climate Coupling by Regional Surveys (SEAC[4]RS) and Deep Convective Clouds and Chemistry Project (DC3) field experiments (Barth et al., 2015; Liu et al., 2013; Zhang et al., 2017). Flight tracks for these experiments were shown in Figure 6. Fresh fire plume data, diagnosed by data points with a correlation coefficient between CO and $CH_3CN > 0.5$ (De Gouw et al., 2004; Liu et al., 2014), were not included in model evaluation as in previous studies.

245   We described in section 3.1 the rationale for sensitivity simulations to evaluate the effects of BrC photo-bleaching and convective wet scavenging. The model sensitivity simulations are listed in Table 2. In the NCNB (base) model, neither effect was included. In the NCB model, the photo-bleaching effect is included. In the ICNB model, the wet scavenging efficiency of BrC was decreased from 75% simulated in the base model to 30%, such that ~70% of BrC was transported through convection to the free troposphere as suggested by Zhang et al. (2016). In the ICB model, both photo-bleaching and reduced
250   convective scavenging effects were included. The ICBB model is similar to ICB model, but photo-bleaching of all BrC was included; in the other models including the phtoto-bleaching effect, only non-convectively transported BrC was affected (Zhang et al., 2017).

Figure 7 shows the observed vertical profiles of BrC absorption to BC ratio (BrC/BC ratio) and concentrations of BC and CO during the DC3 and SEAC⁴RS experiments in comparison to the corresponding model simulation results. The difference between BC and CO vertical profiles is negligible among the sensitivity simulations. Simulated mean BC concentrations are within the uncertainties of the measurements. The underestimation at 2-5 km during SEAC⁴RS suggests transport of non-fire BC to this region since the observed enhancement is insignificant for BrC/BC ratio or CO. The higher CO concentrations in the model than the observations, particularly near the surface, suggests that the model overestimates surface CO emissions.

In the observed profile of BrC/BC shown in Figure 7, BrC/BC increases with the altitude. At 12 km, the BrC/BC ratio is ~10 and ~20 times higher than the BrC/BC near the surface during DC3 and SEAC⁴RS. During DC3 experiment, respectively. Both the observations and model simulations show the increase of BrC/BC ratio at in the upper troposphere. In the sensitivity simulations not including photo-bleaching of BrC (NCNB and ICNB, Table 2), the BrC/BC ratio is higher than the ICB, NCB and ICBB simulations. Non-photo-bleaching simulations overestimate BrC below 5 km in both DC3 and SEAC⁴RS experiments, reflecting the effect of photo-bleaching. In the NCNB simulation, the BrC/BC ratio is underestimated in the upper troposphere (> 8 km). The comparison between simulations with and without convective transport (ICNB&NCNB and ICB&NCB) indicates that deep convective transport increased upper tropospheric BrC/BC ratio compared to the lower troposphere in better agreement with the observed profiles. When photo-bleaching effect of convectively transported BrC is included in the ICBB simulation, the model cannot reproduce the observed enhancement of BrC/BC ratio in the upper troposphere.

The simulation of NCB, which included efficient convective scavenging and photo-bleaching, clearly underestimated the observed BrC/BC ratios in both DC3 and SEAC⁴RS, while the simulation of ICNB, which included reduced convective scavenging but no photo-bleaching, significantly overestimated the BrC/BC ratio observations. The overall best model simulation is ICB, which included reduced convective scavenging and photo-bleaching effect for non-convectively-transported BrC. During the SEAC⁴RS experiment, the BrC/BC in ICB simulation was underestimated in the upper troposphere and overestimated in the middle-lower troposphere. The simulation bias is mostly due to biases in BC simulation in that BC was overestimated in the upper troposphere and underestimated in the middle-lower troposphere (Figure 7). It appears that the model overestimated non-fire BC in the upper troposphere but underestimated non-fire BC in the middle-lower troposphere outside the biomass burning regions. Because the ICB simulation is most consistent with the observations among the model simulations, we applied the ICB model simulation to understand the effects of global BrC radiative forcing.

5.2 Simulated global zonal mean distribution of BrC

285   We performed diagnostic model simulations to investigate the contributions of BrC absorption from biomass burning emissions, biofuel emissions, and secondary formation, respectively. Figure 8 shows the results. Secondary BrC production has a relatively small contribution because of photo-bleaching of secondary BrC is 100%, while a small fraction of BrC is left after photo-bleaching of biomass burning and biofuel BrC (Forrister et al., 2015). Both biofuel and secondary production are largest at northern mid latitudes since they are due to anthropogenic emissions.

290

Biomass burning BrC shows drastically different distributions from biofuel BrC. The latitudinal maximum is in the tropics and subtropics, with a secondary peak at 60°N due to fires over Canada and Siberia. The vertical extent of biomass burning BrC is much higher than biofuel BrC due to fire plume rise (Ke, 2019) and the higher vertical extent of tropical convection than midlatitudes. While the effect of biofuel BrC is primarily in the lower troposphere, the radiative forcing of biomass

295   burning BrC is much more substantial in the free troposphere and therefore more strongly affects the atmosphere since solar heating of the atmosphere is generally weak.

5.3 Global directive radiative effect of BrC

Aerosol DRE represents the instantaneous radiative effect of aerosols, which is sometimes confused with DRF (Heald et al., 2014, Ghan, 2013). We applied the Rapid Radiative Transfer Method for GCMs (RRTMG) to BrC and BC radiative forcing.

300   We parameterized the imaginary part of BrC refractive index as an external input of RRTMG. As discussed in Section 3.2, the imaginary refractive index is specified at 0.045 at 550 nm and 0.043 at 365 nm for primary and secondary BrC, respectively. The wavelength boundaries for RRTMG shortwave and longwave are listed in Tables S1a and S1b in the supplement (Neale et al., 2010; Iacono et al., 2008; Mlawer et al., 1997). We calculated the imaginary refractive index at a different wavelength by introducing wavelength dependence w (Saleh et al., 2014):

305     $$w = AAE - 1, \tag{6}$$

$$k_{BrC,\lambda} = k_{BrC,550} \times \left(\frac{550}{\lambda}\right)^w, \tag{7}$$

where $k_{BrC,\lambda}$ denotes the imaginary refractive index of BrC, and w is the wave-length dependent AAE value. Calculation and parameterization of MAE and the imaginary refraction index of BrC were discussed in Section 3.1.

310

In our estimation of BrC DRE, we only considered the absorption of BrC, and the effect of scattering is not considered. The ICB model calculated global DRE distributions of BrC and BC and the DRE ratio of BrC to BC are shown in Figure 9. For 2010, we estimated the global averaged DRE of BrC absorption at 0.10 W/m² in comparison to 0.39 W/m² by BC. While the global DRE by BrC is less than BC, BrC radiative forcing can be as large as that of BC due to the large difference in

315   emission distributions. BC DRE is large at northern mid latitudes due to anthropogenic emissions from China and India. BrC

emissions are relatively low in these regions (Fig. 1) and consequently BC DRE dominates. Over regions with large fire emissions, both BC and BrC are important. Over most regions of the remote tropical ocean, BrC DRE is larger than BC, suggesting broader regional effects by BrC radiative forcing in the tropics. This simulated feature is due to two factors. In the ICB simulation, wet scavenging removes much more BC than BrC. Therefore, BrC is enriched relative to BC in the free

320   troposphere (e.g., Zhang et. al., 2017). In the tropics, the easterly trade wind in the boundary layer become westerlies in the middle and upper troposphere. The regions of boundary layer BC transport and free tropospheric BrC transport are in opposite directions. As a result, the DRE ratio of BrC to BC is low to the east of the fire emission regions and it is high to the west of the fire emission regions.

325   To discuss our simulation results in the context of previous modeling studies, which did not use the ICB assumptions, we show the annual mean DRE distributions for all model simulations (Table 2) in Figure 10. Comparing the global mean DRE relative change of ICB (0.10 W/m^2) to NCB (0.013 W/m^2) with that of NCNB (0.077 W/m^2) to NCB shows that the global effect of convective scavenging efficiency decrease is larger than photo-bleaching. A similar conclusion can be obtained by comparing the global mean DRE relative change ICNB (0.26 W/m^2) to NCNB with that of ICNB to ICB. The DRE relative

330   change from ICB to ICBB (0.030 W/m^2) indicates the photo-bleaching effect of convectively transported BrC is larger than the enhancement of BrC convective transport. The 0.013 W/m^2 DRE in the NCB simulation agrees with previous model studies considering the photo-bleaching effect (Wang et al., 2018). The 0.077 W/m^2 DRE in the NCNB simulation is comparable to previous studies (Feng et al., 2013; Jo et al., 2016; Wang et al., 2014).

335   Only ICB simulation results are discussed hereafter. Figure 11 shows the seasonally BrC DRE distributions. The seasonal variation is due primarily to biomass burning. Figure 2 shows that the largest fire emissions in August, September, July, and June. While fire emissions are mostly in the tropics in SON, burning at northern mid and high latitudes much more pronounced in JJA in addition to tropical burning.

5.4 Global effects of BrC absorption on the atmosphere

340   As found by Zhang et al. (2017), the importance of radiative heating by BrC relative to BC increases with altitude due to convective transport. We compared the difference of average vertical profiles of BrC to BC heating rate ratio in Figure 13. Over regions directly affected by convection, where the convective mass flux is >10^{-5} kg/m^2/s, the simulated result is in agreement with Zhang et al. (2017). Globally, the average BrC/BC heating rate ratio is >100% at 400 hPa, indicating in deep convection regions, atmospheric heating of BrC is stronger than that of BC. In comparison, over the regions not directly

345   affected by deep convection, the globally averaged BrC/BC heating rate ratio increases from 9% at surface level to 53% in the upper troposphere. Geographically, Figure 14 shows that the difference between BrC and BC is particularly large over the tropics.

The heating rate from aerosols, especially its vertical profile, has significant implications on cloud dynamics (e.g., Bond et
350 al., 2013), and can also induce feedback from regional circulation and the planetary boundary layer dynamics (e.g.,
Ramanathan and Carmichael, 2008). We conducted three 5-year free-running model simulations for the present day (the year
2010). In the control simulation, both BrC and BC heat were included. We then conducted sensitivity simulations in which
only BrC or BC heating was included. By comparing the sensitivity simulation results to the control simulation, we
diagnosed the climate response to differential BrC and BC heating.

355

The latitudinal and vertical difference between BrC and BC heating (Figures 13 and 14) implies that BrC heating is more
dominant in the tropics and tends to decrease the vertical gradient of temperature. Allen et al. (2012) suggested that light-
absorbing aerosols may contribute to tropical expansion. They did not consider the effect of BrC, the atmospheric heating
effect of which is more concentrated in the tropics than BC heating (Figure 14). Using the latitude where the Mean
360 Meridional Circulation (MMC) at 500 hPa becomes zero on the poleward side of the subtropical maximum to diagnose the
boundary of the tropics (Zhou et al., 2011), we estimated a $1.0° \pm 0.9°$ latitude of tropical expansion due to BrC heating in
comparison to a $1.2° \pm 2.9°$ expansion due to BC heating. The large uncertainty comes from 5 years of free-running
simulations and the relatively low model spatial resolution. Another effect from BrC heating is the decrease of deep
convective mass flux over the upper troposphere (Feingold et al., 2005; Yoshimori and Broccoli, 2008). We estimated a
365 decrease of deep convective mass flux by 4.41×10^{-5} $kg/m^2/s$ or 4.1% over the tropics, which is about one-third of the
corresponding BC heating effect (1.52×10^{-4} $kg/m^2/s$ or 12.9%).

Hodnebrog et al. (2016) suggested that biomass burning aerosols suppress precipitation regionally due primarily to aerosol-
cloud interactions. On a global basis, BrC heating reduces precipitation by $0.9\% \pm 7.0\%$, which is about 60% of the
370 precipitation reduction by BC simulated in the model. Over the tropical region with high-intensity convection and
precipitation, BrC heating decreased precipitation by $3.9\% \pm 17.8\%$, similarly to that from BC heating ($4.0\% \pm 17.1\%$). The
effect of BrC heating on tropical precipitation (~100%) is larger than on convective mass flux (~1/3) relative to BC heating
because of the stronger BrC than BC heating in the upper than lower troposphere (Figures 13 and 14). BrC heating decreased
precipitation by $0.3\% \pm 10.7\%$ in the northern mid and high latitudes, which is much lower than the effect of BC heating (-
375 $4.8 \pm 13.5\%$).

6 Conclusions

Light-absorbing aerosols, including BC and BrC, have significant impacts on the global radiative balance. Observational
evidence emerged from the DC3 mission of large enhancements of BrC relative to BC over biomass burning regions (Zhang
et al., 2017). We developed a module of brown carbon in CESM CAM5 and conducted two sets of model experiments, 2010
380 with nudged meteorological fields and 5-year free-running simulations. Evaluations with DC3, SEAC[4]RS, and HIPPO

observations suggested that the model could simulate the observed concentrations of BrC and BC, although model biases were also found. Reducing the convective scavenging efficiency and including photo-bleaching were necessary to simulate the observed BrC distributions. Globally, the former effect is larger than the latter on simulated BrC absorption. Since the two factors have opposite effects on simulated BrC DRE, our best estimation of global DRE of BrC is 0.10 W/m^2, which is

385   comparable to previous studies (Feng et al., 2013; Jo et al., 2016).

The BrC DRE is estimated to be 25% of that of BC. Since biomass burning emissions tend to occur during the warm seasons when solar insolation is strong and these emissions tend to occur in the tropics when convective transport is active, the proportional contribution to BrC DRE by biomass burning emission is larger than its fraction in the total emissions. For

390   example, biofuel BrC emissions are seasonal and occur in mid and high latitudes, the combination of BrC absorption and solar radiation of biofuel BrC is less than biomass burning BrC for a unit of BrC emission. Relative to BC DRE, BrC DRE tends to be larger in the tropics due to different emission distributions and larger BrC levels in the upper troposphere. BrC heating reduces global precipitation by 0.9%, about 60% of the BC induced precipitation decrease. Over the tropics, the reduction of precipitation due to BrC heating is similar to BC heating, but its effect on reducing tropical convective mass

395   flux is only ~1/3 of BC heating because BrC heating is strongly skewed to high altitudes compared to BC heating. Consequently, the effect of BrC heating on tropical expansion is comparable to BC heating.

There are still considerable uncertainties in modeling BrC absorption and its effects in the atmosphere. Emissions, photo-bleaching, and convective transport of BrC all require more field and laboratory observations. The results from this study

400   indicate that field measurements over tropical convective regions during periods of biomass burning are critically needed to further improve our understanding of BrC processes and its climate effects. Continuous model development by coupling BrC related processes and climate effects into an interactive climate-fire-ecosystem model (Zou et al., 2019) in CESM would also benefit future projections of climate radiative forcing given large impacts of fire emitted BrC in the tropics found by this study.

405

Data availability. NASA DC3 and SEAC^{4}RS missions and are available to the general public through the NASA data archive (https://www-air.larc.nasa.gov/cgi-bin/ArcView/dc3 and https://www-air.larc.nasa.gov/cgi-bin/ArcView/seac4rs). MODIS Terra level 3 monthly dataset (MOD08_M3) is available via NASA LAADS Archive (https://ladsweb.modaps.eosdis.nasa.gov/archive/allData/61/MOD08_M3/). HIPPO merged 10-second data is available via

410   CDIAC HIPPO data archive (https://hippo.ornl.gov/data_access). AERONET AOD measurements are available in https://aeronet.gsfc.nasa.gov/new_web/download_all_v3_aod.html. The CAM5 model results are available from the corresponding author upon request.

Competing interests. The authors declare that they have no conflict of interest.

415 *Author contribution.* Yuzhong Zhang and Rodney Weber provided the original idea. Aoxing Zhang, Yuhang Wang and Yufei Zou designed the model experiments. Yongjia Song and Ziming Ke conducted and provided the model input data. Rodney Weber and Yuzhong Zhang conducted and analyzed aircraft measurement data. Aoxing Zhang carried out the model experiments and prepared the manuscript with contributions from all co-authors.

Acknowledgments. This work was supported by the National Science Foundation (NSF) through grant 1243220. we would
420 like to acknowledge high-performance computing support from Cheyenne (Computational and Information Systems Laboratory, 2017) and Yellowstone (ark:/85065/d7w3xhc) provided by National Center for Atmospheric Research (NCAR)'s Computational & Information Systems Lab (CISL), sponsored by the National Science Foundation. We thank Haviland Forrister for helpful discussion.

References

425 Akagi, S., Yokelson, R. J., Wiedinmyer, C., Alvarado, M., Reid, J., Karl, T., Crounse, J., and Wennberg, P.: Emission factors for open and domestic biomass burning for use in atmospheric models, Atmospheric Chemistry and Physics, 11, 4039-4072, https://doi.org/10.5194/acp-11-4039-2011, 2011.

Alexander, D. T., Crozier, P. A., and Anderson, J. R.: Brown carbon spheres in East Asian outflow and their optical properties, Science, 321, 833-836, https://doi.org/ 10.1126/science.1155296, 2008

430 Allen, R. J., Sherwood, S. C., Norris, J. R., and Zender, C. S.: Recent Northern Hemisphere tropical expansion primarily driven by black carbon and tropospheric ozone, Nature, 485, 350-354, https://doi.org/10.1038/nature11097, 2012

Ångström, A.: The parameters of atmospheric turbidity, Tellus, 16, 64-75, 1964.

Barth, M. C., Cantrell, C. A., Brune, W. H., Rutledge, S. A., Crawford, J. H., Huntrieser, H., Carey, L. D., MacGorman, D., Weisman, M., Pickering, K. E. and Bruning, E.: The deep convective clouds and chemistry (DC3) field campaign. Bulletin
435 of the American Meteorological Society, 96(8), 1281-1309, https://doi.org/10.1175/BAMS-D-13-00290.1, 2015.

Bond, T. C., and Bergstrom, R. W.: Light absorption by carbonaceous particles: An investigative review, Aerosol science and technology, 40, 27-67, https://doi.org/10.1080/02786820500421521, 2006

Bond, T. C., Bhardwaj, E., Dong, R., Jogani, R., Jung, S., Roden, C., Streets, D. G., and Trautmann, N. M.: Historical emissions of black and organic carbon aerosol from energy-related combustion, 1850–2000, Global Biogeochemical Cycles,
440 21, https://doi.org/10.1029/2006GB002840, 2007.

Bond, T. C., Doherty, S. J., Fahey, D., Forster, P., Berntsen, T., DeAngelo, B., Flanner, M., Ghan, S., Kärcher, B., and Koch, D.: Bounding the role of black carbon in the climate system: A scientific assessment, Journal of Geophysical Research: Atmospheres, 118, 5380-5552, https://doi.org/10.1002/jgrd.50171, 2013.

Bretherton, C. S., and Park, S.: A new moist turbulence parameterization in the Community Atmosphere Model, Journal of
445 Climate, 22, 3422-3448, https://doi.org/10.1175/2008JCLI2556.1, 2009.

Brown, H., Liu, X., Feng, Y., Jiang, Y., Wu, M., Lu, Z., Wu, C., Murphy, S. and Pokhrel, R., 2018. Radiative effect and climate impacts of brown carbon with the Community Atmosphere Model (CAM5). Atmospheric Chemistry and Physics, 18, 17745-17768, https://doi.org/10.5194/acp-18-17745-2018, 2018.

Browne, E. C., Zhang, X., Franklin, J. P., Ridley, K. J., Kirchstetter, T. W., Wilson, K. R., Cappa, C. D., and Kroll, J. H.:

450   Effect of heterogeneous oxidative aging on light absorption by biomass-burning organic aerosol, Aerosol Science and Technology, 1-15, https://doi.org/10.1080/02786826.2019.1599321, 2019.

Chakrabarty, R., Moosmüller, H., Chen, L.-W., Lewis, K., Arnott, W., Mazzoleni, C., Dubey, M., Wold, C., Hao, W., and Kreidenweis, S.: Brown carbon in tar balls from smoldering biomass combustion, Atmospheric Chemistry and Physics, 10, 6363-6370, https://doi.org/ 10.5194/acp-10-6363-2010, 2010.

455   Cheng, Y., He, K.-B., Zheng, M., Duan, F.-K., Du, Z.-Y., Ma, Y.-L., Tan, J.-H., Yang, F.-M., Liu, J.-M., and Zhang, X.-L.: Mass absorption efficiency of elemental carbon and water-soluble organic carbon in Beijing, China, Atmospheric Chemistry and Physics, 11, 11497-11510, https://doi.org/10.5194/acp-11-11497-2011, 2011.

Chipperfield, M.: New version of the TOMCAT/SLIMCAT off-line chemical transport model: Intercomparison of stratospheric tracer experiments, Quarterly Journal of the Royal Meteorological Society, 132, 1179-1203,

460   https://doi.org/10.1256/qj.05.51, 2006.

Computational and Information Systems Laboratory: Cheyenne: HPE/SGI ICE XA System (University Community Computing). Boulder, CO: National Center for Atmospheric Research. https://doi.org/10.5065/D6RX99HX, 2017

Costabile, F., Gilardoni, S., Barnaba, F., Ianni, A. D., Liberto, L. D., Dionisi, D., Manigrasso, M., Paglione, M., Poluzzi, V., and Rinaldi, M.: Characteristics of brown carbon in the urban Po Valley atmosphere, Atmospheric Chemistry and Physics,

465   17, 313-326, https://doi.org/10.5194/acp-17-313-2017, 2017.

De Gouw, J., Cooper, O., Warneke, C., Hudson, P., Fehsenfeld, F., Holloway, J., Hübler, G., Nicks Jr, D., Nowak, J., and Parrish, D.: Chemical composition of air masses transported from Asia to the US West Coast during ITCT 2K2: Fossil fuel combustion versus biomass-burning signatures, Journal of Geophysical Research: Atmospheres, 109, https://doi.org/10.1029/2003JD004202, 2004.

470   Desyaterik, Y., Sun, Y., Shen, X., Lee, T., Wang, X., Wang, T., and Collett, J. L.: Speciation of "brown" carbon in cloud water impacted by agricultural biomass burning in eastern China, Journal of Geophysical Research: Atmospheres, 118, 7389-7399, https://doi.org/10.1002/jgrd.50561, 2013.

Di Lorenzo, R. A., and Young C. J.: Size separation method for absorption characterization in brown carbon: Application to an aged biomass burning sample, Geophys. Res. Lett., 43, 458-465, https://doi.org/10.1002/2015GL066954, 2015.

475   Di Lorenzo, R. A., Washenfelder R. A., Attwood, A. R., Guo, H., Xu, L., Ng, S., Weber, R. J., Baumann, K., Edgerton, E., and Young, C. J.: Molecular-Size-Separated Brown Carbon Absorption for Biomass-Burning Aerosol at Multiple Field Sites, Envir. Sci. Technol, 51, 3128-3137, 2017.Feingold, G., Jiang, H., and Harrington, J. Y.: On smoke suppression of clouds in Amazonia, Geophysical Research Letters, 32, https://doi.org/10.1029/2004GL021369, 2005.

Feng, Y., Ramanathan, V., and Kotamarthi, V. R.: Brown carbon: a significant atmospheric absorber of solar radiation?,
480   Atmospheric Chemistry and Physics, 13, 8607-8621, https://doi.org/10.5194/acp-13-8607-2013, 2013.

Fernandes, S. D., Trautmann, N. M., Streets, D. G., Roden, C. A., and Bond, T. C.: Global biofuel use, 1850–2000, Global
Biogeochemical Cycles, 21, https://doi.org/10.1029/2006GB002836, 2007.

Forrister, H., Liu, J., Scheuer, E., Dibb, J., Ziemba, L., Thornhill, K. L., Anderson, B., Diskin, G., Perring, A. E., and
Schwarz, J. P.: Evolution of brown carbon in wildfire plumes, Geophysical Research Letters, 42, 4623-4630,
485   https://doi.org/10.1002/2015GL063897, 2015.

Gettelman, A., Liu, X., Ghan, S. J., Morrison, H., Park, S., Conley, A., Klein, S. A., Boyle, J., Mitchell, D., and Li, J. L.:
Global simulations of ice nucleation and ice supersaturation with an improved cloud scheme in the Community Atmosphere
Model, Journal of Geophysical Research: Atmospheres, 115, https://doi.org/10.1029/2009JD013797, 2010.

Ghan, S. J., Liu, X., Easter, R. C., Zaveri, R., Rasch, P. J., Yoon, J.-H., and Eaton, B.: Toward a minimal representation of
490   aerosols in climate models: Comparative decomposition of aerosol direct, semidirect, and indirect radiative forcing, Journal
of Climate, 25, 6461-6476, https://doi.org/10.1175/JCLI-D-11-00650.1, 2012.

Ghan, S. J.: Technical Note: Estimating aerosol effects on cloud radiative forcing, Atmospheric Chemistry and Physics, 13,
9971-9974, https://doi.org/10.5194/acp-13-9971-2013, 2013.

Giglio, L., Randerson, J. T., and Werf, G. R.: Analysis of daily, monthly, and annual burned area using the fourth-generation
495   global fire emissions database (GFED4), Journal of Geophysical Research: Biogeosciences, 118, 317-328,
https://doi.org/10.1002/jgrg.20042, 2013.

Heald, C.L., Ridley, D.A., Kroll, J.H., Barrett, S.R.H., Cady-Pereira, K.E., Alvarado, M.J. and Holmes, C.D.: Contrasting
the direct radiative effect and direct radiative forcing of aerosols. Atmospheric Chemistry and Physics, 14, 5513-5527,
https://doi.org/10.5194/acp-14-5513-2014, 2013.

500   Hecobian, A., Zhang, X., Zheng, M., Frank, N., Edgerton, E. S., and Weber, R. J.: Water-Soluble Organic Aerosol material
and the light-absorption characteristics of aqueous extracts measured over the Southeastern United States, Atmospheric
Chemistry and Physics, 10, 5965-5977, https://doi.org/10.5194/acp-10-5965-2010, 2010.

Hodnebrog, Ø., Myhre, G., Forster, P. M., Sillmann, J., and Samset, B. H.: Local biomass burning is a dominant cause of the
observed precipitation reduction in southern Africa, Nature communications, 7, https://doi.org/10.1038/ncomms11236, 2016.

505   Holben, B. N., Eck, T., Slutsker, I., Tanre, D., Buis, J., Setzer, A., Vermote, E., Reagan, J., Kaufman, Y., and Nakajima, T.:
AERONET—A federated instrument network and data archive for aerosol characterization, Remote sensing of environment,
66, 1-16, https://doi.org/10.1016/S0034-4257(98)00031-5, 1998.

Iacono, M. J., Delamere, J. S., Mlawer, E. J., Shephard, M. W., Clough, S. A., and Collins, W. D.: Radiative forcing by long-
lived greenhouse gases: Calculations with the AER radiative transfer models, Journal of Geophysical Research:
510   Atmospheres, 113, https://doi.org/10.1029/2008JD009944, 2008.

Jacobson, M. Z.: Isolating nitrated and aromatic aerosols and nitrated aromatic gases as sources of ultraviolet light
absorption, Journal of Geophysical Research: Atmospheres, 104, 3527-3542, https://doi.org/10.1029/1998JD100054, 1999.

Jo, D. S., Park, R. J., Lee, S., Kim, S.-W., and Zhang, X.: A global simulation of brown carbon: implications for photochemistry and direct radiative effect, Atmospheric Chemistry and Physics, 16, 3413-3432, https://doi.org/10.5194/acp-16-3413-2016, 2016.

515

Junker, C., and Liousse, C.: A global emission inventory of carbonaceous aerosol from historic records of fossil fuel and biofuel consumption for the period 1860–1997, Atmospheric Chemistry and Physics, 8, 1195-1207, https://doi.org/10.5194/acp-8-1195-2008, 2008.

Ke, Z.: The Global Plume-rise Dataset and Its Climate Model Implement, in preparation, 2019.

520

Kirchstetter, T., and Thatcher, T.: Contribution of organic carbon to wood smoke particulate matter absorption of solar radiation, Atmospheric Chemistry and Physics, 12, 6067-6072, https://doi.org/10.5194/acp-12-6067-2012, 2012.

Kirchstetter, T. W., Novakov, T., and Hobbs, P. V.: Evidence that the spectral dependence of light absorption by aerosols is affected by organic carbon, Journal of Geophysical Research: Atmospheres, 109, https://doi.org/10.1029/2004JD004999, 2004.

525

Kumar, K. R., Sivakumar, V., Reddy, R., Gopal, K. R., and Adesina, A. J.: Inferring wavelength dependence of AOD and Ångström exponent over a sub-tropical station in South Africa using AERONET data: Influence of meteorology, long-range transport and curvature effect, Science of the Total Environment, 461, 397-408, https://doi.org/10.1016/j.scitotenv.2013.04.095, 2013.

Lamarque, J.-F., Bond, T. C., Eyring, V., Granier, C., Heil, A., Klimont, Z., Lee, D., Liousse, C., Mieville, A., and Owen,

530

B.: Historical (1850–2000) gridded anthropogenic and biomass burning emissions of reactive gases and aerosols: methodology and application, Atmospheric Chemistry and Physics, 10, 7017-7039, https://doi.org/10.5194/acp-10-7017-2010, 2010.

Lambe, A. T., Cappa, C. D., Massoli, P., Onasch, T. B., Forestieri, S. D., Martin, A. T., Cummings, M. J., Croasdale, D. R., Brune, W. H., and Worsnop, D. R.: Relationship between oxidation level and optical properties of secondary organic

535 aerosol, Environmental science & technology, 47, 6349-6357, https://doi.org/10.1021/es401043j, 2013.

Laskin, A., Laskin, J., and Nizkorodov, S. A.: Chemistry of atmospheric brown carbon, Chemical reviews, 115, 4335-4382, https://doi.org/10.1021/cr5006167, 2015.

Laskin, J., Laskin, A., Nizkorodov, S. A., Roach, P., Eckert, P., Gilles, M. K., Wang, B., Lee, H. J., and Hu, Q.: Molecular selectivity of brown carbon chromophores, Environmental science & technology, 48, 12047-12055,

540 https://doi.org/10.1021/es503432r, 2014.

Lavi, A., Lin, P., Bhaduri, B., Carmieli, R., Laskin, A., and Rudich, Y.: Characterization of light-absorbing oligomers from reactions of phenolic compounds and Fe (III), ACS Earth and Space Chemistry, 1, 637-646, https://doi.org/10.1021/acsearthspacechem.7b00099, 2017.

Lee, H. J., Aiona, P. K., Laskin, A., Laskin, J., and Nizkorodov, S. A.: Effect of solar radiation on the optical properties and

545 molecular composition of laboratory proxies of atmospheric brown carbon, Environmental science & technology, 48, 10217-10226, https://doi.org/10.1021/es502515r, 2014.

Lin, G., Penner, J. E., Flanner, M. G., Sillman, S., Xu, L., and Zhou, C.: Radiative forcing of organic aerosol in the atmosphere and on snow: Effects of SOA and brown carbon, Journal of Geophysical Research: Atmospheres, 119, 7453-7476, https://doi.org/10.1002/2013JD021186, 2014.

550   Lin, P., Liu, J., Shilling, J. E., Kathmann, S. M., Laskin, J., and Laskin, A.: Molecular characterization of brown carbon (BrC) chromophores in secondary organic aerosol generated from photo-oxidation of toluene, Physical Chemistry Chemical Physics, 17, 23312-23325, https://doi.org/10.1039/C5CP02563J, 2015.

Liu, J., Fan, S., Horowitz, L. W., and Levy, H.: Evaluation of factors controlling long-range transport of black carbon to the Arctic, Journal of Geophysical Research: Atmospheres, 116, https://doi.org/10.1029/2010JD015145, 2011.

555   Liu, J., Bergin, M., Guo, H., King, L., Kotra, N., Edgerton, E., and Weber, R.: Size-resolved measurements of brown carbon in water and methanol extracts and estimates of their contribution to ambient fine-particle light absorption, Atmospheric Chemistry and Physics, 13, 12389-12404, https://doi.org/10.5194/acp-13-12389-2013, 2013.

Liu, J., Scheuer, E., Dibb, J., Ziemba, L. D., Thornhill, K., Anderson, B. E., Wisthaler, A., Mikoviny, T., Devi, J. J., and Bergin, M.: Brown carbon in the continental troposphere, Geophysical Research Letters, 41, 2191-2195,
560   https://doi.org/10.1002/2013GL058976, 2014.

Liu, J., Lin, P., Laskin, A., Laskin, J., Kathmann, S. M., Wise, M., Caylor, R., Imholt, F., Selimovic, V., and Shilling, J. E.: Optical properties and aging of light-absorbing secondary organic aerosol, Atmospheric Chemistry and Physics, 16, 12815-12827, https://doi.org/10.5194/acp-16-12815-2016, 2016.

Liu, X., Easter, R. C., Ghan, S. J., Zaveri, R., Rasch, P., Shi, X., Lamarque, J.-F., Gettelman, A., Morrison, H., and Vitt, F.:
565   Toward a minimal representation of aerosols in climate models: Description and evaluation in the Community Atmosphere Model CAM5, Geoscientific Model Development, 5, 709, https://doi.org/10.5194/gmd-5-709-2012, 2012.

Ma, P. L., Rasch, P. J., Wang, H., Zhang, K., Easter, R. C., Tilmes, S., Fast, J. D., Liu, X., Yoon, J. H., and Lamarque, J. F.: The role of circulation features on black carbon transport into the Arctic in the Community Atmosphere Model version 5 (CAM5), Journal of Geophysical Research: Atmospheres, 118, 4657-4669, https://doi.org/10.1002/jgrd.50411, 2013.

570   Magalhães, A. C. O., Esteves da Silva, J. C., and Pinto da Silva, L. s.: Density functional theory calculation of the absorption properties of brown carbon chromophores generated by catechol heterogeneous ozonolysis, ACS Earth and Space Chemistry, 1, 353-360, https://doi.org/10.1021/acsearthspacechem.7b00061, 2017.

McMeeking, G. R.: The optical, chemical, and physical properties of aerosols and gases emitted by the laboratory combustion of wildland fuels, Colorado State University, 2008.

575   Mlawer, E. J., Taubman, S. J., Brown, P. D., Iacono, M. J., and Clough, S. A.: Radiative transfer for inhomogeneous atmospheres: RRTM, a validated correlated-k model for the longwave, Journal of Geophysical Research: Atmospheres, 102, 16663-16682, http://doi.org/10.1029/97JD00237, 1997.

Morrison, H., and Gettelman, A.: A new two-moment bulk stratiform cloud microphysics scheme in the Community Atmosphere Model, version 3 (CAM3). Part I: Description and numerical tests, Journal of Climate, 21, 3642-3659,
580   https://doi.org/10.1175/2008JCLI2105.1, 2008.

Nakayama, T., Matsumi, Y., Sato, K., Imamura, T., Yamazaki, A., and Uchiyama, A.: Laboratory studies on optical properties of secondary organic aerosols generated during the photooxidation of toluene and the ozonolysis of α-pinene, Journal of Geophysical Research: Atmospheres, 115, https://doi.org/10.1029/2010JD014387, 2010.

Nakayama, T., Sato, K., Matsumi, Y., Imamura, T., Yamazaki, A., and Uchiyama, A.: Wavelength and NO x dependent complex refractive index of SOAs generated from the photooxidation of toluene, Atmospheric Chemistry and Physics, 13, 531-545, https://doi.org/10.5194/acp-13-531-2013, 2013.

Neale, R. B., Chen, C.-C., Gettelman, A., Lauritzen, P. H., Park, S., Williamson, D. L., Conley, A. J., Garcia, R., Kinnison, D., and Lamarque, J.-F.: Description of the NCAR community atmosphere model (CAM 5.0), NCAR Tech. Note NCAR/TN-486+ STR, 2010.

Nguyen, T. B., Lee, P. B., Updyke, K. M., Bones, D. L., Laskin, J., Laskin, A., and Nizkorodov, S. A.: Formation of nitrogen-and sulfur-containing light-absorbing compounds accelerated by evaporation of water from secondary organic aerosols, Journal of Geophysical Research: Atmospheres, 117, http://doi.org/10.1029/2011JD016944, 2012.

Odum, J. R., Jungkamp, T., Griffin, R. J., Forstner, H., Flagan, R. C., and Seinfeld, J. H.: Aromatics, reformulated gasoline, and atmospheric organic aerosol formation, Environmental Science & Technology, 31, 1890-1897, https://doi.org/10.1021/es960535l, 1997.

Park, R. J., Kim, M. J., Jeong, J. I., Youn, D., and Kim, S.: A contribution of brown carbon aerosol to the aerosol light absorption and its radiative forcing in East Asia, Atmospheric environment, 44, 1414-1421, https://doi.org/10.1016/j.atmosenv.2010.01.042, 2010.

Park, S., and Bretherton, C. S.: The University of Washington shallow convection and moist turbulence schemes and their impact on climate simulations with the Community Atmosphere Model, Journal of Climate, 22, 3449-3469, https://doi.org/10.1175/2008JCLI2557.1, 2009.

Pillar, E. A., Camm, R. C., and Guzman, M. I.: Catechol oxidation by ozone and hydroxyl radicals at the air–water interface, Environmental science & technology, 48, 14352-14360, https://doi.org/10.1021/es504094x, 2014.

Pillar, E. A., and Guzman, M. I.: Oxidation of substituted catechols at the air–water interface: Production of carboxylic acids, quinones, and polyphenols, Environmental science & technology, 51, 4951-4959, https://doi.org/10.1021/acs.est.7b00232, 2017.

Platnick, S., et al.: MODIS Atmosphere L3 Monthly Product. NASA MODIS Adaptive Processing System, Goddard Space Flight Center, USA, http://dx.doi.org/10.5067/MODIS/MOD08_M3.061, 2017

Ramanathan, V., and Carmichael, G.: Global and regional climate changes due to black carbon, Nature geoscience, 1, 221-227, https://doi.org/10.1038/ngeo156, 2008.

Randerson, J., Chen, Y., Werf, G., Rogers, B., and Morton, D.: Global burned area and biomass burning emissions from small fires, Journal of Geophysical Research: Biogeosciences, 117, https://doi.org/10.1029/2012JG002128, 2012.

Richter, J. H., and Rasch, P. J.: Effects of convective momentum transport on the atmospheric circulation in the Community Atmosphere Model, version 3, Journal of Climate, 21, 1487-1499, https://doi.org/10.1175/2007JCLI1789.1, 2008.

615 Saleh, R., Robinson, E. S., Tkacik, D. S., Ahern, A. T., Liu, S., Aiken, A. C., Sullivan, R. C., Presto, A. A., Dubey, M. K., and Yokelson, R. J.: Brownness of organics in aerosols from biomass burning linked to their black carbon content, Nature Geoscience, 7, 647-650, https://doi.org/10.1038/ngeo2220, 2014.

Saleh, R., Marks, M., Heo, J., Adams, P. J., Donahue, N. M., & Robinson, A. L.: Contribution of brown carbon and lensing to the direct radiative effect of carbonaceous aerosols from biomass and biofuel burning emissions. Journal of Geophysical

620 Research: Atmospheres, 120(19), https://doi.org/10.1002/ 2015JD023697, 2015.

Sareen, N., Moussa, S. G., and McNeill, V. F.: Photochemical aging of light-absorbing secondary organic aerosol material, The Journal of Physical Chemistry A, 117, 2987-2996, https://doi.org/10.1021/jp309413j, 2013.

Schuster, G., Dubovik, O., and Arola, A.: Remote sensing of soot carbon–Part 1: Distinguishing different absorbing aerosol species, Atmospheric Chemistry and Physics, 16, 1565-1585, https://doi.org/10.5194/acp-16-1565-2016, 2016a.

625 Schuster, G., Dubovik, O., Arola, A., Eck, T., and Holben, B.: Remote sensing of soot carbon–Part 2: Understanding the absorption Ångström exponent, Atmospheric Chemistry and Physics, 16, 1587-1602, https://doi.org/10.5194/acp-16-1587-2016, 2016b.

Schwarz, J., Spackman, J., Gao, R., Watts, L., Stier, P., Schulz, M., Davis, S., Wofsy, S., and Fahey, D.: Global-scale black carbon profiles observed in the remote atmosphere and compared to models, Geophysical Research Letters, 37,

630 https://doi.org/10.1029/2010GL044372, 2010.

Schwarz, J., Samset, B., Perring, A., Spackman, J., Gao, R., Stier, P., Schulz, M., Moore, F., Ray, E. A., and Fahey, D.: Global-scale seasonally resolved black carbon vertical profiles over the Pacific, Geophysical research letters, 40, 5542-5547, https://doi.org/10.1002/2013GL057775, 2013.

Smith, J. D., Kinney, H., and Anastasio, C.: Phenolic carbonyls undergo rapid aqueous photodegradation to form low-

635 volatility, light-absorbing products, Atmospheric environment, 126, 36-44, https://doi.org/10.1016/j.atmosenv.2015.11.035, 2016.

Stohl, A., Klimont, Z., Eckhardt, S., Kupiainen, K., Shevchenko, V. P., Kopeikin, V., and Novigatsky, A.: Black carbon in the Arctic: the underestimated role of gas flaring and residential combustion emissions, Atmospheric Chemistry and Physics, 13, 8833-8855, https://doi.org/10.5194/acp-13-8833-2013, 2013.

640 Rienecker, M., Suarez, M. J., Todling, R., Bacmeister, J., Takacs, L., Liu, H., Gu, W., Sienkiewicz, M., Koster, R., Gelaro, R., Stajner, I., and Nielsen, J.: The GEOS-5 Data Assimilation System-Documentation of Versions 5.0. 1, 5.1. 0, and 5.2. 0, 2008.

Updyke, K. M., Nguyen, T. B., and Nizkorodov, S. A.: Formation of brown carbon via reactions of ammonia with secondary organic aerosols from biogenic and anthropogenic precursors, Atmospheric Environment, 63, 22-31,

645 https://doi.org/10.1016/j.atmosenv.2012.09.012, 2012.

Wang, H., Easter, R. C., Rasch, P. J., Wang, M., Liu, X., Ghan, S. J., Qian, Y., Yoon, J.-H., Ma, P.-L., and Vinoj, V.: Sensitivity of remote aerosol distributions to representation of cloud–aerosol interactions in a global climate model, Geoscientific Model Development, 6, 765-782, https://doi.org/10.5194/gmd-6-765-2013, 2013.

Wang, M., Ghan, S., Easter, R., Ovchinnikov, M., Liu, X., Kassianov, E., Qian, Y., Gustafson Jr, W., Larson, V., and
650 Schanen, D.: The multi-scale aerosol-climate model PNNL-MMF: Model description and evaluation, Geoscientific Model
Development, 4, 137, https://doi.org/10.5194/gmd-4-137-2011, 2011.

Wang, X., Heald, C., Ridley, D., Schwarz, J., Spackman, J., Perring, A., Coe, H., Liu, D., and Clarke, A.: Exploiting
simultaneous observational constraints on mass and absorption to estimate the global direct radiative forcing of black carbon
and brown carbon, Atmospheric Chemistry and Physics, 14, 10989-11010, https://doi.org/10.5194/acp-14-10989-2014.
655 2014.

Wang, X., Heald, C. L., Liu, J., Weber, R. J., Campuzano-Jost, P., Jimenez, J. L., Schwarz, J. P., and Perring, A. E.:
Exploring the observational constraints on the simulation of brown carbon, Atmospheric Chemistry and Physics, 18, 635,
https://doi.org/10.5194/acp-18-635-2018, 2018.

Ward, D. S., Kloster, S., Mahowald, N. M., Rogers, B. M., Randerson, J. T., and Hess, P. G.: The changing radiative forcing
660 of fires: global model estimates for past, present and future, Atmospheric Chemistry and Physics, 12, 10857-10886,
https://doi.org/10.5194/acp-12-10857-2012, 2012.

Washenfelder, R., Attwood, A., Brock, C., Guo, H., Xu, L., Weber, R., Ng, N., Allen, H., Ayres, B., and Baumann, K.:
Biomass burning dominates brown carbon absorption in the rural southeastern United States, Geophysical Research Letters,
42, 653-664, https://doi.org/10.1002/2014GL062444, 2015.

665 Wofsy, S. C.: HIAPER Pole-to-Pole Observations (HIPPO): fine-grained, global-scale measurements of climatically
important atmospheric gases and aerosols, Philosophical Transactions of the Royal Society of London A: Mathematical,
Physical and Engineering Sciences, 369, 2073-2086, https://doi.org/10.1098/rsta.2010.0313, 2011.

Wong, J. P. S., Nenes. A., and Weber, R. J., Changes in light absorptivity of molecular weight separated brown carbon due
to photolytic aging, Envir. Sci. Technol, 51, 8414-8421, https://doi.org/10.1021/acs.est.7b01739, 2017.

670 Wong, J. P. S., Tsgaraki, M., Tsiodra, I., Mihalopoulos, N., Vilaki, K., Kanakidou, M., Sciare, J., Nenes, A., and Weber, R.
J., Atmospheric evolution of molecular weight separated brown carbon from biomass burning, Atm. Chem. Phys., 19, 7319-
7334, https://doi.org/10.5194/acp-19-7319-2019 2019.

Xie, M., Hays, M. D., and Holder, A. L.: Light-absorbing organic carbon from prescribed and laboratory biomass burning
and gasoline vehicle emissions, Scientific Reports, 7, 7318, https://doi.org/10.1038/s41598-017-06981-8, 2017.

675 Yan, C., Zheng, M., Bosch, C., Andersson, A., Desyaterik, Y., Sullivan, A. P., Collett, J. L., Zhao, B., Wang, S., and He, K.:
Important fossil source contribution to brown carbon in Beijing during winter, Scientific Reports, 7, 43182,
https://doi.org/10.1038/srep43182, 2017.

Yang, M., Howell, S., Zhuang, J., and Huebert, B.: Attribution of aerosol light absorption to black carbon, brown carbon,
and dust in China–interpretations of atmospheric measurements during EAST-AIRE, Atmospheric Chemistry and Physics, 9,
680 2035-2050, https://doi.org/10.5194/acp-9-2035-2009, 2009.

Yoshimori, M., and Broccoli, A. J.: Equilibrium response of an atmosphere–mixed layer ocean model to different radiative forcing agents: Global and zonal mean response, Journal of Climate, 21, 4399-4423, https://doi.org/10.1175/2008JCLI2172.1, 2008.

685 Yu, L., Smith, J., Laskin, A., George, K. M., Anastasio, C., Laskin, J., Dillner, A. M., and Zhang, Q.: Molecular transformations of phenolic SOA during photochemical aging in the aqueous phase: competition among oligomerization, functionalization, and fragmentation, Atmospheric Chemistry and Physics, 16, 4511-4527, 2016.

Zhang, G., and McFarlane, N. A.: Sensitivity of climate simulations to the parameterization of cumulus convection in the Canadian Climate Centre general circulation model, Atmosphere-ocean, 33, 407-446, https://doi.org/10.1080/07055900.1995.9649539, 1995.

690 Zhang, Q., Streets, D. G., Carmichael, G. R., He, K., Huo, H., Kannari, A., Klimont, Z., Park, I., Reddy, S., and Fu, J.: Asian emissions in 2006 for the NASA INTEX-B mission, Atmospheric Chemistry and Physics, 9, 5131-5153, https://doi.org/10.5194/acp-9-5131-2009, 2009.

Zhang, X., Lin, Y. H., Surratt, J. D., Zotter, P., Prévôt, A. S., and Weber, R. J.: Light-absorbing soluble organic aerosol in Los Angeles and Atlanta: A contrast in secondary organic aerosol, Geophysical Research Letters, 38,
695 https://doi.org/10.1029/2011GL049385, 2011.

Zhang, Y., Forrister, H., Liu, J., Dibb, J., Anderson, B., Schwarz, J. P., Perring, A. E., Jimenez, J. L., Campuzano-Jost, P., and Wang, Y.: Top-of-atmosphere radiative forcing affected by brown carbon in the upper troposphere, Nature Geoscience, 10, 486, https://doi.org/10.1038/ngeo2960, 2017.

Zhao, R., Lee, A., Huang, L., Li, X., Yang, F., and Abbatt, J.: Photochemical processing of aqueous atmospheric brown
700 carbon, Atmospheric Chemistry and Physics, 15, 6087-6100, https://doi.org/10.5194/acp-15-6087-2015, 2015.

Zhong, M., and Jang, M.: Light absorption coefficient measurement of SOA using a UV–Visible spectrometer connected with an integrating sphere, Atmospheric environment, 45, 4263-4271, https://doi.org/10.1016/j.atmosenv.2011.04.082, 2011.

Zhong, M., Jang, M., Oliferenko, A., Pillai, G. G., and Katritzky, A. R.: The SOA formation model combined with semiempirical quantum chemistry for predicting UV-Vis absorption of secondary organic aerosols, Physical Chemistry
705 Chemical Physics, 14, 9058-9066, https://doi.org/10.1039/c2cp23906j, 2012.

Zhou, Y., Xu, K. M., Sud, Y., and Betts, A.: Recent trends of the tropical hydrological cycle inferred from Global Precipitation Climatology Project and International Satellite Cloud Climatology Project data, Journal of Geophysical Research: Atmospheres, 116, https://doi.org/10.1029/2010JD015197, 2011.

Zou, Y., Wang, Y., Ke, Z., Tian, H., Yang, J., and Liu, Y.: Development of a REgion-Specific Ecosystem Feedback Fire
710 (RESFire) Model in the Community Earth System Model, Journal of Advances in Modeling Earth Systems, 11, 417-445, https://doi.org/10.1029/2018MS001368, 2019.

Table 1. BrC emission sources (TgC yr⁻¹) of this and previous studies.

	This work	Jo et. al. (2016)	Wang et al. (2014)
Primary biomass burning source	3.6	3.0±1.7	
Primary biofuel source	3.1	3.0±1.3	8 for primary sources
Secondary formation	4.1	5.7	3.2

715

720

Table 2. BrC sensitivity simulations

CAM run name	NCNB (base model)	ICNB	NCB	ICBB	ICB (best model)
Reduced BrC convective wet scavenging	No	Yes	No	Yes	Yes
Photo-bleaching of convective transported BrC	No	No	Yes	Yes	No
Photo-bleaching of non- convective transported BrC	No	No	Yes	Yes	Yes

725

730
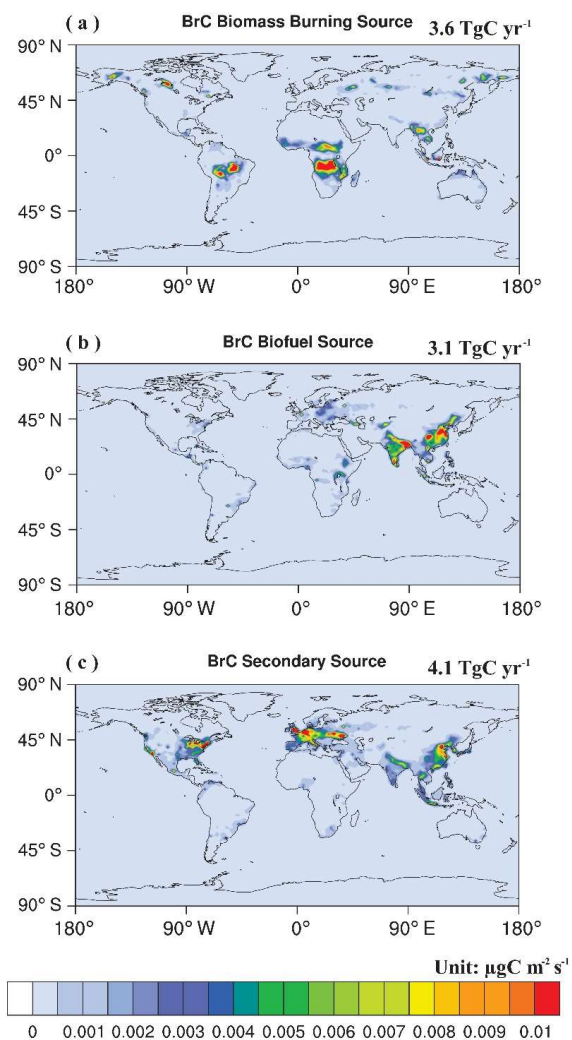
Figure 1. Spatial distributions of global emissions of BrC from biomass burning (a), anthropogenic biofuel combustion (b) and secondary formation (c) in 2010. Unit is μg C m^{-2} s^{-1}. The total emission is 3.6, 3.1, and 4.1 Tg C yr^{-1} for biomass burning, biofuel, and secondary formation, respectively.

735
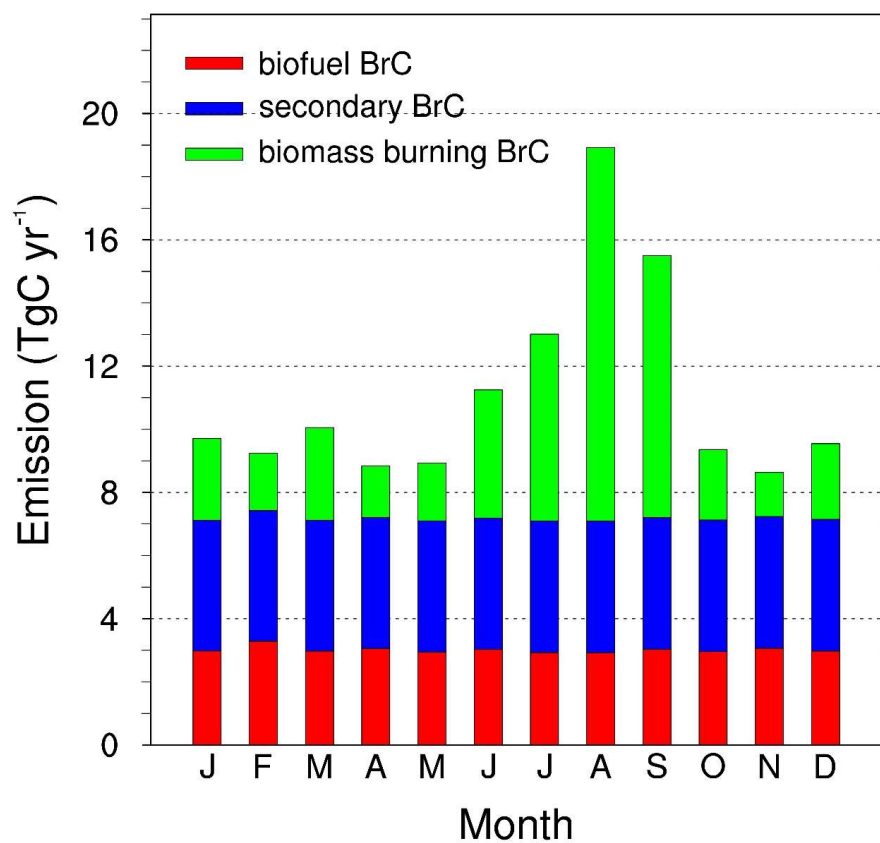
Figure 2. Monthly mean global BrC emission rates (Tg C yr^{-1}) in 2010. Green, blue, and red bars represent the emissions from biomass burning, biofuel combustion, and secondary BrC formation, respectively.

740
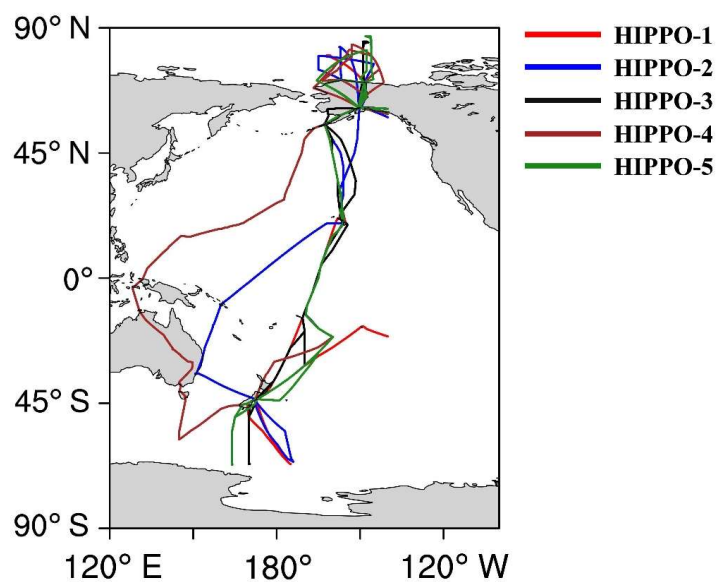
Figure 3. Flight track of the 5 HIPPO missions. Colored lines in red, blue, black, brown, green represent flight track of HIPPO-1 to HIPPO-5 respectively. Flights over continental North America east of 140°W were not included in this study.

745
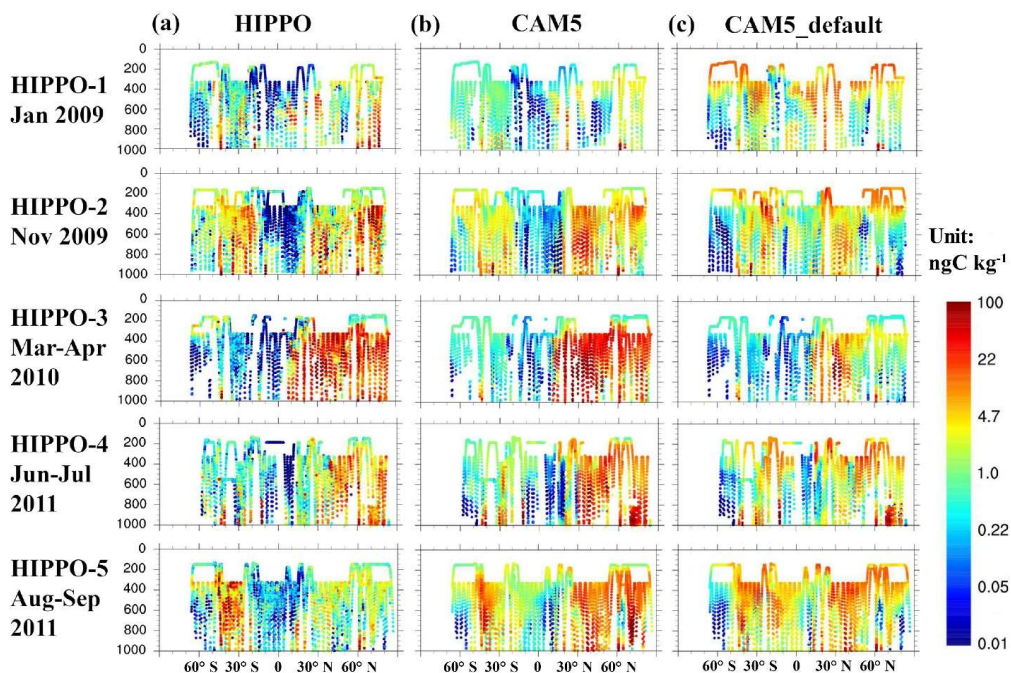
Figure 4. Comparison of HIPPO BC (ng C kg⁻¹) measurements (a), simulated BC data from the modified CAM5 model (b) and simulated BC data from the default CAM5 model (c) during HIPPO mission 1-5. The 5 rows from top to bottom are HIPPO-1 (Jan 2009), HIPPO-2 (Nov, 2009), HIPPO-3 (Mar-Apr, 2010), HIPPO-4 (Jun-Jul, 2011), and HIPPO-5 (Aug-Sep, 2011), respectively. Measurement data along the flight tracks of Fig. 3 are 1-min averages. Model data are selected corresponding to the location and time of aircraft measurements.
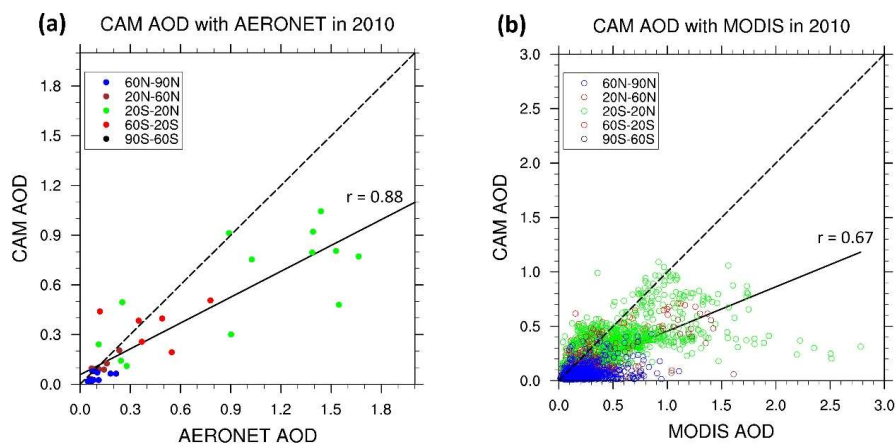
Figure 5. Comparison of monthly mean AOD data in 550 nm for fire dominated months and regions (Figure S1(a)) of model simulations with observations for 2010, (a) AERONET and (b) MODIS. Model data correspond to the same time and location of the observations. The data points are color-coded as a function of latitude. The solid line denotes a least-squares regression and the dashed line denotes the 1:1 reference line.

755

760

765
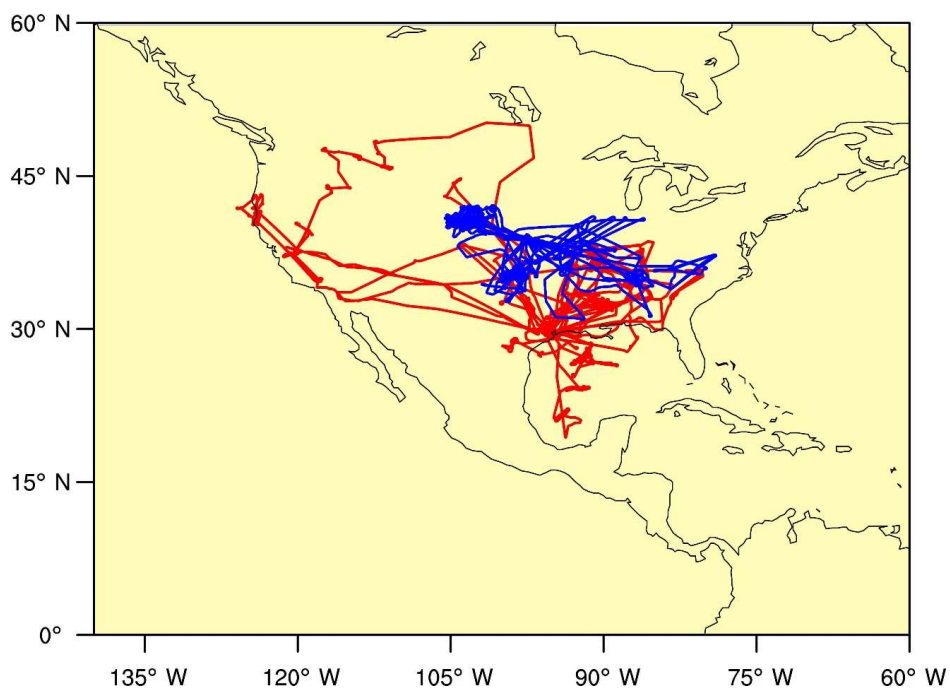
Figure 6. Flight tracks of DC3 (red) and SEAC⁴RS (blue) field experiments.

770
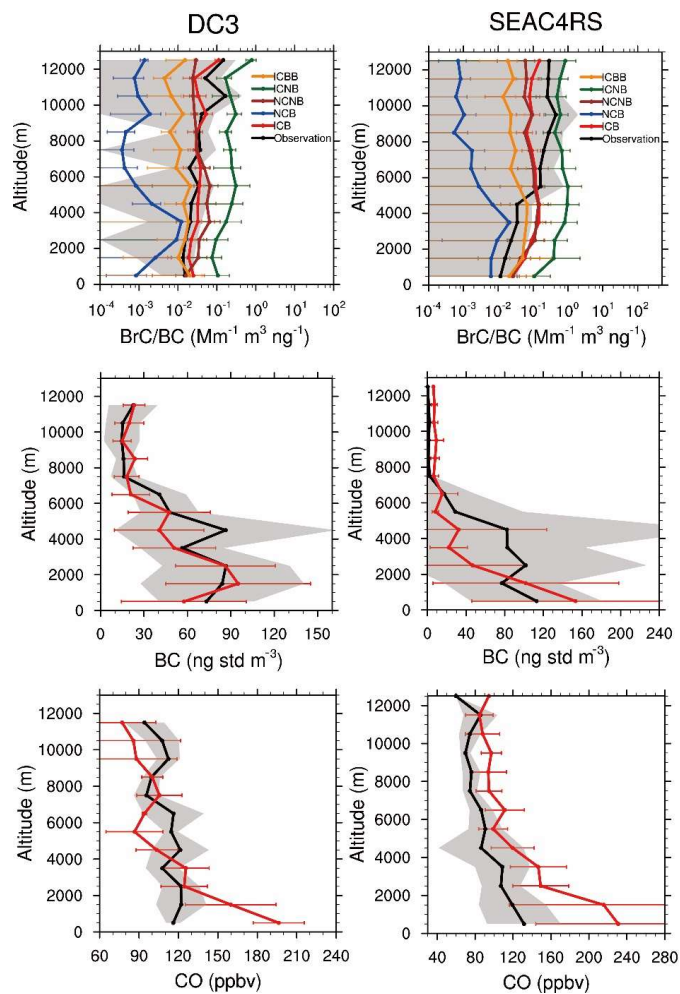
Figure 7. Comparison between observed and simulated vertical profiles of the ratio between BrC absorption at 365 nm and BC (top), and concentrations of BC (middle) and CO (bottom) for the DC3 (left column) and SEAC⁴RS (right column) missions. Black lines and shaded areas show the means and standard deviations of the observations binned in 1-km intervals, respectively. The colored vertical lines and horizontal bars show the means and standard deviations of corresponding model results, respectively. Model sensitivity simulations of BrC are listed in Table 2. The difference among simulated BC and CO vertical profiles is negligible and the ICB simulation results are shown.

780
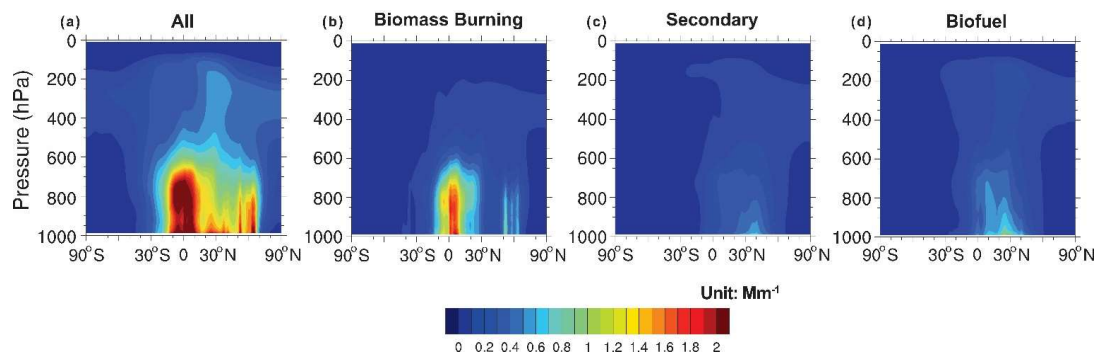
Figure 8. Simulated zonal averaged annual mean BrC absorption at 365 nm (Mm^{-1}) for (a) all sources, (b) biomass burning emissions, (c) secondary BrC formation, and (d) biofuel BrC emissions. Unit is Mm^{-1}. Color bar is in log scale.
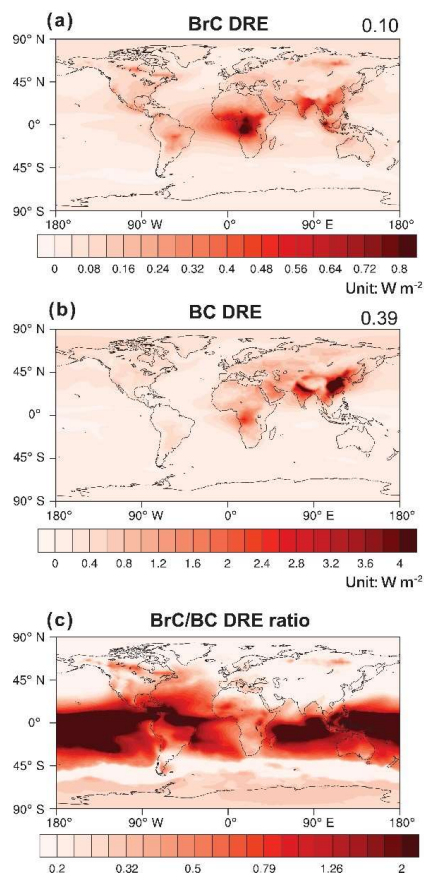
Figure 9. Annual averaged global distributions of (a) BC DRE, (b) BrC DRE, and (c) ratio of BrC/BC DRE for 2010. The unit is W m⁻². The global averaged DRE is shown in the upper right corner.
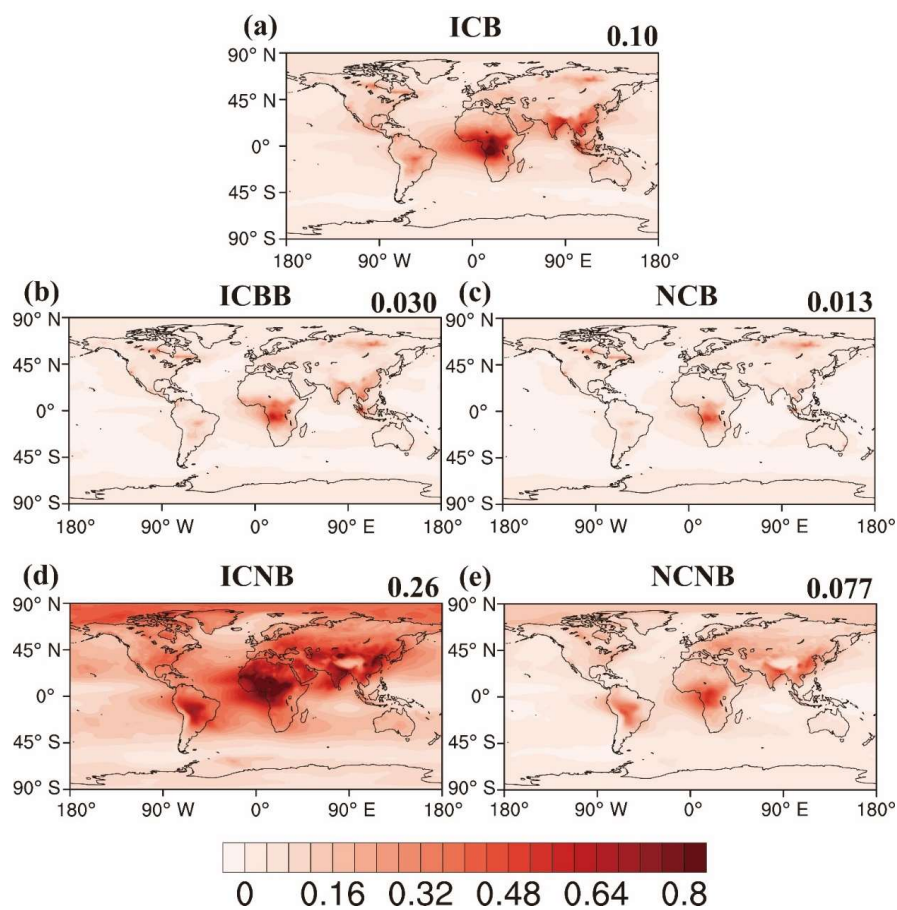
785

Figure 10. Annual averaged global distributions of BrC DRE for all sensitivity simulations (Table 2). The unit is W m^{-2}. The global averaged DRE is shown in the upper right corner.
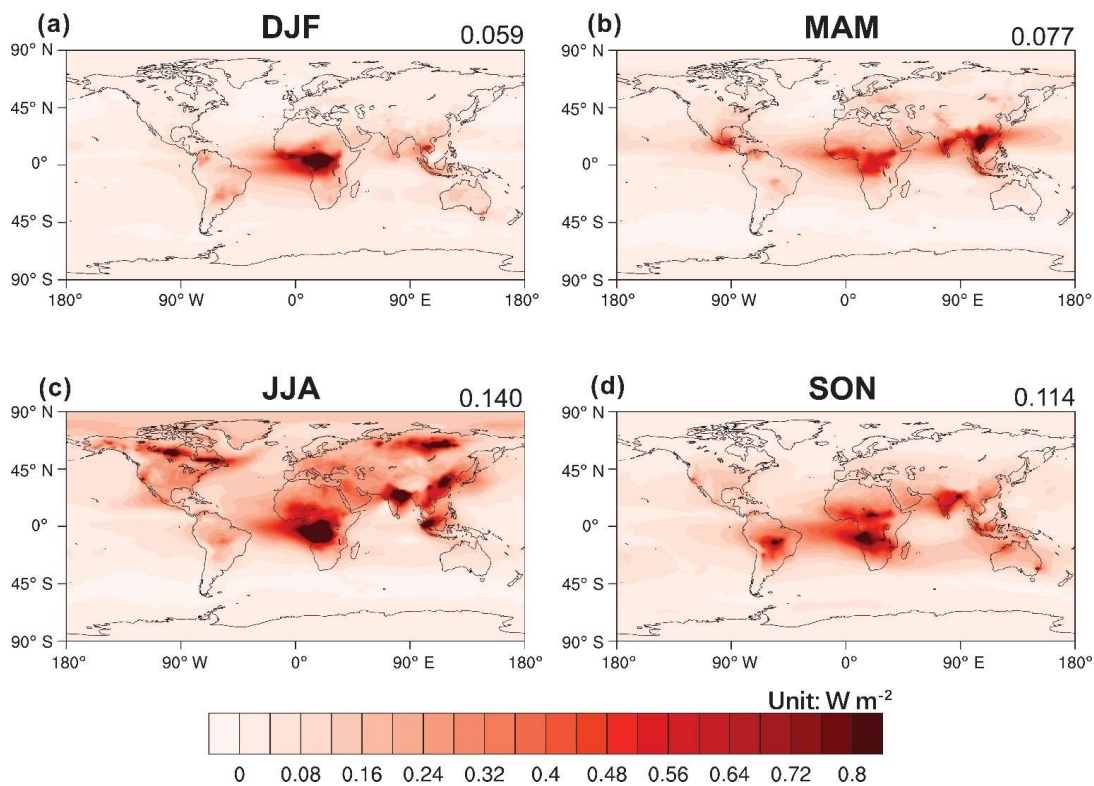
790

Figure 11. Same as Fig. 10 but for seasonal global DRE distributions of BrC for (a) DJF, (b) MAM, (c) JJA, (d) SON in the ICB simulation.
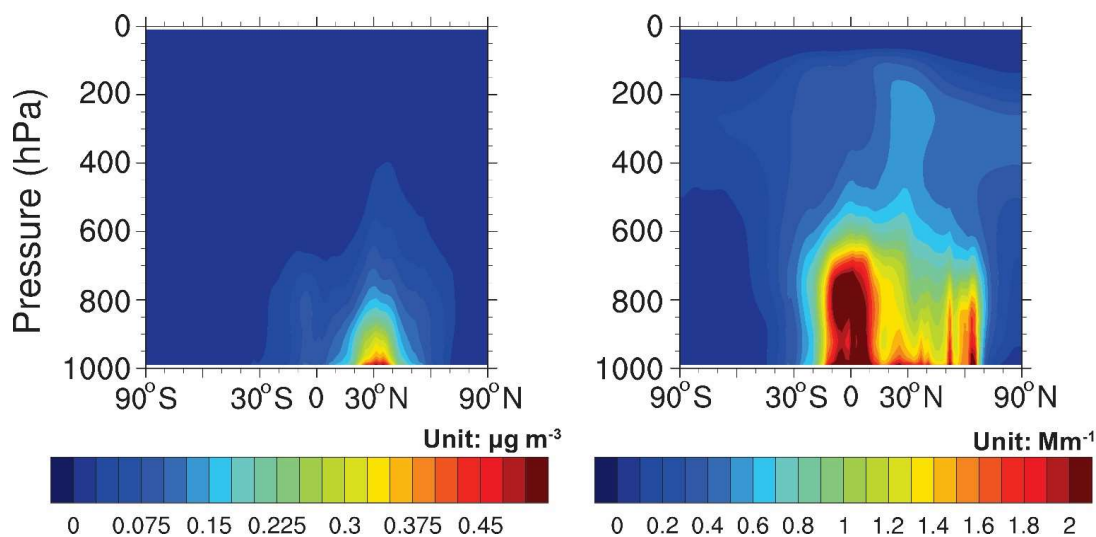
Figure 12. Global zonal mean distributions of (a) BC mass concentrations (μg std m⁻³) and (b) BrC absorption at 365 nm (Mm⁻¹) for 2010.
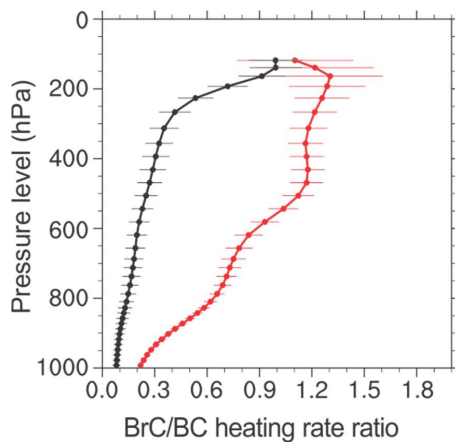
Figure 13. Global averaged vertical profile of BrC toBC heating rate ratio for 2010. The black and red lines are the average profiles for regions without and with deep convection events, respectively. Standard deviations are indicated by the horizontal bars.

795

800
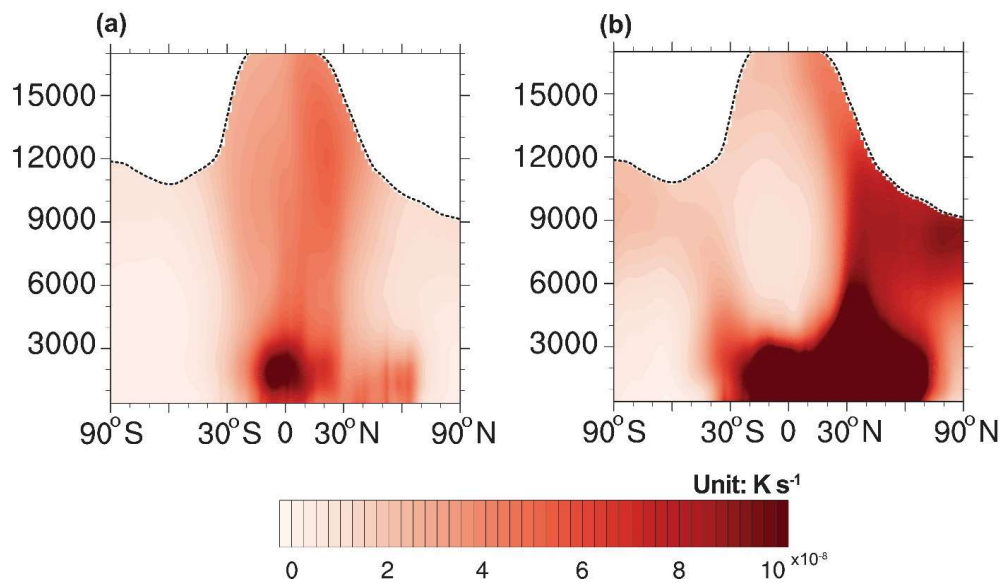
Figure 14. Global zonal mean distributions of heating rate of (a) BrC and (b) BC for 5 years of present-day simulations. The dash line denotes the tropopause.

805